https://doi.org/10.5194/egusphere-2026-5873
Preprint. Discussion started: 18 November 2026
© Author(s) 2026. CC BY 4.0 License.

Bedform-scale controls on dense-grain concentration, sorting, and escape: Where should geoscientists sample dense tracers in bedform deposits?

Max Daniller-Varghese[1, now at 2], David Mohrig[1], and Wonsuck Kim[1, now at 3]

[1]The University of Texas at Austin, Jackson School of Geosciences, Department of Geosciences, Austin, TX
[2]The University of Texas at Austin, Applied Research Laboratories, Austin, TX
[3]Yonsei University, Department of Earth System Sciences, Seoul, South Korea

Correspondence: Max Daniller-Varghese (maxdv@utexas.edu)

Abstract. The provenance of sedimentary basins is commonly determined using the spectra of radioactive decay products within dense tracer grains (e.g. detrital zircons) and matching these spectra against basement rock. In this paper we report the results of experiments that investigate the transport mechanisms of dense grains (magnetite) within a less-dense bulk sediment load of quartz sand. Our question is: to what degree do dense tracers reflect the transport histories of bulk quartz sediment? And, are the tracer grains' concentration, size distribution, and sorting a function of differing modes of sediment transport? To investigate this, we measured the concentration and size distributions of dense particles preserved within the body of experimentally generated subaqueous sand dunes. This paper aims to establish an understanding of the mechanics of sediment transport in a detrital zircon context. Using a set of experiments, we show the lagging process of dense grains associated with movement of a single unidirectional bedform, and develop a simple set of sampling principles to choose dense tracer grains that represent bulk sediment in various transport settings.

1 Introduction

Zircon is a common accessory mineral in siliciclastic sediment. This mineral contains up to one part in a hundred of radioactive U and Th, which decay into products with known half-lives, forming the basis of the $U-Th-Pb$ geochronometer. Because zircon grains are so durable chemically and physically, they are considered an excellent and representative "fingerprint" of their source rock (Vermeesch, 2012).

Detrital zircon geochronology has become one of the primary tools for linking sedimentary deposits to their source rocks (Fedo et al., 2003; Gehrels, 2014). Detrital zircon age distributions have been used in a myriad of ways, and have grown in popularity in recent decades to identify sediment sources, reconstruct sediment-routing systems, test paleogeographic connections, track drainage reorganization, constrain the timing of exhumation and unroofing, and recognize sediment recycling through basin histories (Coutts et al., 2019; Sharman and Malkowski, 2020). These applications depend on the premise that zircon age spectra are a meaningful source signal as grains are transferred from source terranes, through transport systems, and into preserved deposits.

https://doi.org/10.5194/egusphere-2026-5873
Preprint. Discussion started: 18 November 2026
© Author(s) 2026. CC BY 4.0 License.

Applications of detrital zircon geochronology assume that the statistical metrics measuring dissimilarity between samples can be used to determine distinct sedimentary sources (Saylor and Sundell, 2016; Vermeesch, 2018; Ibañez-Mejia et al., 2018). However, provenance studies consistently show that detrital zircon $U - Pb$ ages are also correlated to grain size (Sircombe et al., 2001; Garzanti et al., 2009; Lawrence et al., 2011; Ibañez-Mejia et al., 2018). The local size distribution of sediment changes along the length of a single bedform, but this principle of bedform transport-filtering has yet to be applied to detrital zircon sampling strategies. Moreover, numerous studies have demonstrated how sediment transport is strongly dependent on grain size, shape, and density (Stokes, 1851; Udden, 1914; Shields, 1936; Rouse, 1937; Dietrich, 1982; Viparelli et al., 2015). Notably, Ibañez-Mejia et al. (2018) found that simple significance testing of samples is insufficient to determine whether a sediment sample is truly derived from multiple sources, or a single source transport-lagged in time. This uncertainty represents an opportunity to integrate traditional sediment transport relationships into detrital zircon studies, including the application of grain transportability into age estimates and investigating the transport filtering effect that bedforms have on dense grains.

Conceptually, the connections between local grain-size distribution and sediment transport across a bedform are summarized in Figure 1. At a given location, grains of different densities, sizes, and shapes will exhibit different behaviors at different rates, and when these propensities are integrated over a long time and a large spatial scale, they can introduce heterogeneity in a sedimentary system. If the style of transport and the transport histories for bulk sediment and tracer grains are different, then the tracer may not faithfully represent bulk sediment. One problem that may arise is overestimating ages or misidentifying an age provenance because the dense tracers' transport time is different enough to skew an age distribution.

Once buried or stored outside the active transport layer, a sediment grain does not reflect the instantaneous transport conditions of the system. This matters for detrital-zircon interpretation because using the youngest grains as a proxy for depositional age assumes that crystallization, exhumation, transport, and deposition occur rapidly, but modern sediment systems show that young zircon can be rare, diluted, selectively transported, or absent even where active sources exist (Malkowski et al., 2019; Sharman and Malkowski, 2020; Dobbs et al., 2022).

To explore the boundary conditions of differential transport at the meso-scale (a fluvial bedform), we used an ensemble of physical experiments that bracket a range of transport regimes from bedload transport to incipient suspension of the finer part of the quartz population. After a predetermined stopping condition, translating the bedform one wavelength, we determine the transport difference of dense tracer particles relative to bulk quartz sediment. We hypothesize that bedforms filter dense tracer grains in predictable ways. Bedload-dominated transport will produce upstream enrichment of dense grains, higher-flow transport will shift dense-grain enrichment toward the crestline, and the dense grains that escape the bedform will be finer than those retained as lag.

2 Methods

2.1 Experimental Methods

Experiments were conducted in the Experimental Sedimentology Lab at the University of Texas at Austin, using an $11\,m$ long recirculating flume (Figure 2). The flume was $0.6\,m$ wide and $1.2\,m$ deep. Using a flow diffuser at the upstream end,

https://doi.org/10.5194/egusphere-2026-5873
Preprint. Discussion started: 18 November 2026
© Author(s) 2026. CC BY 4.0 License.

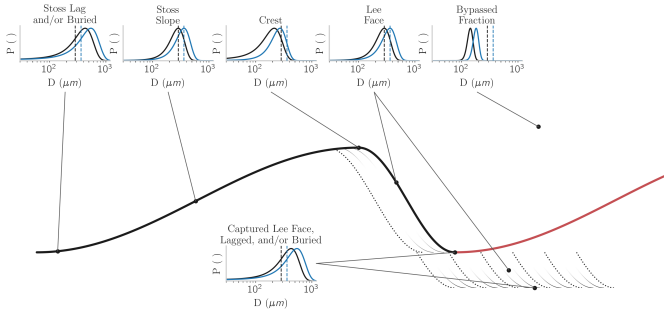


Figure 1. A conceptual diagram of the transport and sorting processes operating across a migrating bedform. The nominal grain size distributions of a bulk sediment (in black) and the dense tracer (in blue) relative to the bulk median value (vertical dashed lines) are plotted across different locations of a bedform. Grains can be transported up the stoss slope, recycled through the body of the bedform, avalanched down the lee face, buried, re-exhumed, or ejected into suspension near the crestline. These pathways are not always equivalent for all grains. Coarser or denser grains are more likely to be retained as lag on the stoss side or captured within lee-side deposits. Finer, less dense grains are more mobile and are more likely to reach the crestline, pass over the lee face, or enter suspended load. As a result, preserved bedforms can contain many transport subpopulations: retained lag grains, recycled bedform grains, crestline-enriched grains, lee-face deposits, and escaped or suspended grains.

logarithmic flow-velocity profiles were generated, measured by a Nortek Aquadopp Acoustic Doppler Profiler. One meter from the flow diffuser, a $2\,m$ long by $50\,mm$ thick bed of sand was smoothed to cover the base of the flume (Figure 4, top row). The sand mixture included $90\,kg$ of medium quartz sand, $D_{50} = 281\,\mu m$, $\rho_{qtz} = 2616\,kg/m^3$ and $1\,kg$ of magnetic sediment, $D_{50} = 330\,\mu m$, $\rho_{mag} = 4990\,kg/m^3$. This tracer concentration was chosen so that it was measurable within the bulk sediment.

To explore a range of environmental conditions, flow was varied to create several transport conditions (Table 1): both sands moving as bedload at a low transport rate (Experiment 5); both sands moving as bedload at higher rates (Experiments 4, 6, 3, and 7); and higher-flow conditions in which the median quartz and magnetic grains remain bedload-dominated, while a larger fraction of the finer quartz population has a propensity for suspension (Experiments 2 and 8). These transport conditions are characterized by the dimensionless Rouse number (Rouse, 1937):

$$P = \frac{w_s}{\kappa u_{sf}}, \tag{1}$$

where w_s is the settling velocity of the grain (m/s), u_{sf} is the skin-friction shear velocity of the flow (m/s), and κ is a dimensionless von Kármán constant, 0.4. Values below 2.5 nominally represent suspension, and values above are varying degrees of bedload transport. These thresholds describe the modeled transport propensity of a grain size, not direct observation that the entire sediment load is suspended.

https://doi.org/10.5194/egusphere-2026-5873
Preprint. Discussion started: 18 November 2026
© Author(s) 2026. CC BY 4.0 License.

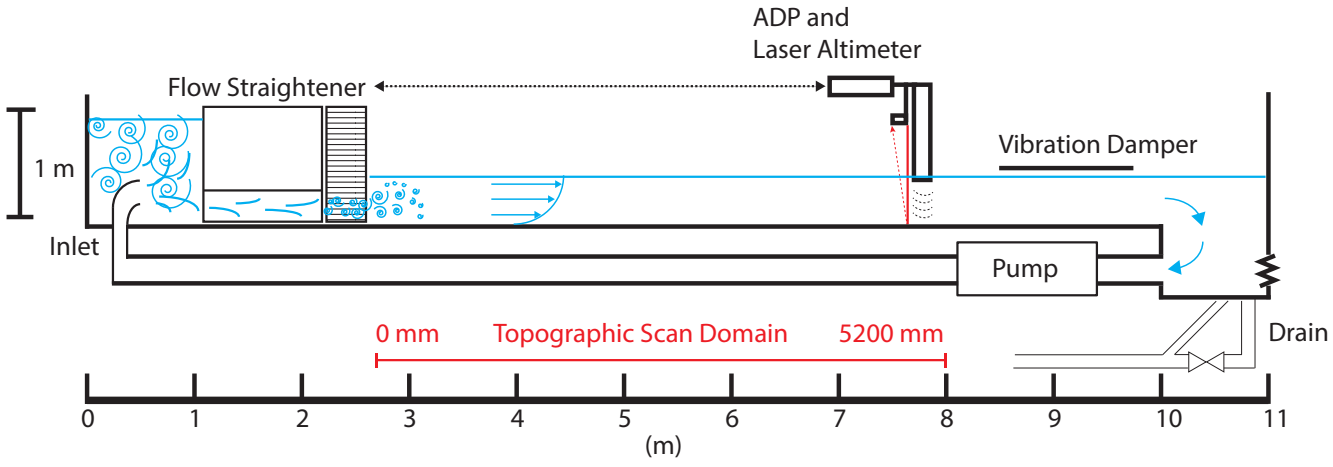


Figure 2. A vertically exaggerated schematic of the experimental setup: The Long Flume in the Experimental Sedimentology Lab at the University of Texas at Austin. The flume measures $11\,m$ long, $1.2\,m$ deep, and $0.6\,m$ wide.

Because of the sensitivity of grain transport to flow velocity, we found that some finer grains of each sediment type approached or entered the suspension-propensity range, even though the median grains remained bedload-dominated, and were able to also transport both as only bedload, which is expanded upon in the Results and Discussion sections. The mean vertically averaged flow velocities associated with the four transport conditions were $0.136 m/s$ (Experiment 5), $0.149 m/s$ (Experiments 4 and 6), $0.163\,m/s$ (Experiments 3 and 7), and $0.179\,m/s$ (Experiments 2 and 8). Despite a modest range in mean flow velocities between the experiments, we were able to generate a range of transport rates for the median quartz sediment, and theoretical transport conditions (based on the derived Rouse numbers, and retained volume fraction, Table 1) because our experiments operated at thresholds for different types of transport. Our experiments were paused periodically throughout their duration to take elevation scans of the deposits.

The experiments were run until the bedform translated one full wavelength past its initial deposition location (Figure 4). This does not ensure that complete steady-state transport filtering occurred, but by enforcing the rule of every grain in the domain necessarily experiencing at least one transport event we had some assurance that aggregate transportability was being modeled by the experiment.

After the transport conditions were satisfied, hand samples were taken. After draining the tank, samples were taken at $0.25 m$ intervals along the centerline of the deposit. A $0.5 l$ plastic cup, $92 mm$ in diameter, was inserted into the bed from the top of the deposit to the base of the flume to include the entire sediment column in the sample. These samples were dried in an oven before the dense, magnetic sediment was separated out of the samples with a magnet. Each dry sample was spread thinly over a pan, and a strong ceramic magnet wrapped in plastic was repeatedly drawn through the sediment, extracting the dense, magnetic grains. When tested as a method for particle extraction, this method was able to extract at a minimum $1\,g$ of magnetic material

https://doi.org/10.5194/egusphere-2026-5873
Preprint. Discussion started: 18 November 2026
© Author(s) 2026. CC BY 4.0 License.

Table 1. Experiments organized by input mean flow velocity. Derived bedload flux, skin-friction shear velocity, volume retention relative to the second scan, Rouse number for the median quartz and magnetic grains, and excess transport stage are reported. The excess transport stage is $T = (u_{sf}/u_c)^2 - 1$, where u_{sf} is the inferred skin-friction shear velocity and u_c is the critical shear velocity for the median grain size of the respective sediment.

Exp.	Mean Flow Vel., $\overline{u}$, $(\mathrm{m\,s^{-1}})$	Bedload Flux, q_b, $(\mathrm{m^2\,s^{-1}})$	Skin-Friction Shear Vel., u_{sf}, $(\mathrm{m\,s^{-1}})$	Vol. Frac. Ret.	Rouse Num., Med. Qtz., $\frac{w_s}{\kappa u_{sf}}$	Rouse Num., Med. Mag., $\frac{w_s}{\kappa u_{sf}}$	Qtz. $T = (\frac{u_{sf}}{u_c})^2 - 1$	Mag. $T = (\frac{u_{sf}}{u_c})^2 - 1$
2	17.86e-02	14.05e-06	3.37e-02	0.893	2.57 (Bedload)	6.44 (Bedload)	5.205	1.469
8	17.86e-02	7.73e-06	2.92e-02	0.811	2.97 (Bedload)	7.45 (Bedload)	3.645	0.848
3	16.28e-02	12.68e-06	3.29e-02	0.963	2.64 (Bedload)	6.61 (Bedload)	4.897	1.347
7	16.28e-02	6.68e-06	2.82e-02	0.852	3.07 (Bedload)	7.70 (Bedload)	3.342	0.728
4	14.93e-02	4.60e-06	2.59e-02	0.973	3.34 (Bedload)	8.38 (Bedload)	2.674	0.462
6	14.93e-02	4.95e-06	2.63e-02	0.999	3.29 (Bedload)	8.24 (Bedload)	2.793	0.509
5	13.61e-02	2.72e-06	2.32e-02	0.896	3.72 (Bedload)	9.34 (Bedload)	1.953	0.175

out of $1\,kg$ of sediment, values approximately an order of magnitude below those measured in the experimental samples. The magnetic and non-magnetic samples were then weighed to determine their mass concentrations.

A Retsch CAMSIZER, Model P4, optical grain size analyzer was used to determine the grain size. The quartz sediment was placed in a vibrating chute, which poured sediment in a plane parallel to a high speed camera that photographed the sediment. The instrument determines the grain size distribution of the sediment using this data.

Because the magnetic sediment has an "effective cohesion," its grain size could not be analyzed on its own. The magnetic force between the grains causes them to clump, and skew the distribution to appear coarser than it actually was. To remedy this, each magnetic sand sample was mixed with glass spheres with a known, narrow size distribution ($D_{50} = 175\,\mu m$, $\sigma = 0.15$, Very Well sorted). This mixture effectively disaggregated the magnetic sand. The grain size distribution was determined by subtracting the known glass spheres' distribution from the combined distribution. The 99.9th percentile of the glass spheres was $255\,\mu m$, and was used as a high-pass filter for interpolating the cumulative distribution functions of the dense, magnetic sediment for all experiments (Figure 3).

2.2 Modeling Grain Transport

2.2.1 Inverse Modeling Skin Friction

Beginning with the known sediment transport conditions measured in the flume, we determine the stress required to transport the sediment measured in the experiments (Table 1). Rather than estimating parameters from fluid flow, we can directly determine the bed stress that transported the sediment in the experiments.

https://doi.org/10.5194/egusphere-2026-5873
Preprint. Discussion started: 18 November 2026
© Author(s) 2026. CC BY 4.0 License.

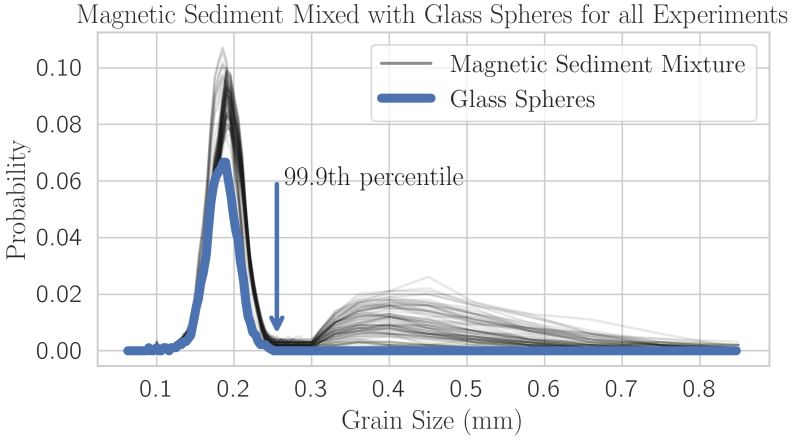


Figure 3. Magnetic sediment samples were mixed with narrowly sorted glass spheres. This disaggregated the cohesive magnetic grains before grain-size analysis. The 99.9th percentile of the glass-sphere distribution, 255 μm, was used as a high-pass cutoff for isolating and interpolating the dense sediment grain-size distributions.

The component of the bed shear stress, τ_{sf} (Pa), affecting sediment transport is referred to as "skin friction stress." Skin friction stress is only a small component of the total boundary shear stress exerted by the flow,

$$\tau_b = \tau_{sf} + \tau_{fd}, \tag{2}$$

where τ_b (Pa) is the total boundary shear stress (Nelson and Smith, 1989; Mohrig and Smith, 1996; Nittrouer et al., 2011). The form drag stress, τ_{fd} (Pa), is the component of the total stress associated with the roughness elements on the channel bed like grains, dunes, and topography. We calculate the skin friction stress values from the known, measured, bedload flux, q_b (m^2/s).

Bedload transport is related to the difference between the skin friction stress and the critical shear stress required to move the median sediment of the bed. These terms are non-dimensionalized by the following:

$$\tau^* = \frac{\tau}{(\rho_s - \rho_f) g D_{50}}, \tag{3}$$

where ρ_s is sediment density (kg/m^3), ρ_f is fluid density (kg/m^3), g is gravitational acceleration (m/s^2), and D_{50} is the median grain size (m).

The bedload transport rate of sediment with a single mode can be described by the relationship relating the exceedance of stress relative to the critical stress required for sediment motion, τ_c^*:

$$q_b^* = \gamma(\tau_{sf}^* - \tau_c^*)^{1.5} \tag{4}$$

where q_b^* relates to the bedload sediment per unit width of flow q_b as,

$$q_b^* = \frac{q_b}{\sqrt{(RgD_{50}^3)}}. \tag{5}$$

https://doi.org/10.5194/egusphere-2026-5873
Preprint. Discussion started: 18 November 2026
© Author(s) 2026. CC BY 4.0 License.

R is the submerged specific gravity of the sediment ($(\rho_s - \rho_f)/\rho_f$). The exceedance threshold is modified by a parameter γ, first proposed by Meyer-Peter and Muller in 1948, and has been frequently modified depending on the composition of sediment. Wiberg and Rubin (1989), and Mohrig and Smith (1996), allow γ to vary as a function of the non-dimensional skin friction stress,

$$\gamma = 1.6 \ln(\tau^*_{sf}) + 9.8. \tag{6}$$

Combining this free term, γ, in Equation 6, with the non-dimensional bedload flux, q^*_b, from Equation 5, and the non-dimensional skin friction stress, τ^*, in Equation 3, and inputting them into Equation 4, we can determine the required skin friction stress for the sediment transport we observe in each experiment. We invert measured bedform-translation flux for the skin-friction stress required to sustain it. We determine the shear velocity at the bed with the following:

$$u_{sf} = \sqrt{\frac{\tau_{sf}}{\rho_f}}. \tag{7}$$

The values for each experiment are reported in Table 1; as transport increases, so does shear velocity.

2.2.2 Suspended Sediment Potential and Escape from the Bedform

A grain is considered to be in suspended load when the fluid column dominates transport conditions, and the settling velocity of the grain becomes the relevant driving parameter limiting transport. Bedload is defined as grains transporting by rolling, sliding or saltating along the bed. Quartz grains that enter suspension can be carried downstream beyond the migrating bedform, while less mobile dense grains remain within or behind it. Consequently, transport associated with bedform migration need not represent the total sediment flux. As previously mentioned in the Methods, the ratio between the settling velocity and the shear velocity (Equation 1), characterizes transport type of a particular grain size. The settling velocity formulation used was derived by Ferguson and Church (2004):

$$w_s = \frac{(RgD_n^2)}{C_1\nu + (0.75 C_2 RgD_n^3)^{0.5}}, \tag{8}$$

where C_1 and C_2 are parameterized values of 20 and 1.1 for natural grains using the nominal diameter (Ferguson and Church (2004), and ν is a kinematic viscosity ($1.004 \times 10^{-6}\, m^2/s$), fitting Dietrich (1982) for natural grains).

With our inverse model-derived shear velocities (Equation 7, Table 1), and the calculated settling velocity from each grain (Equation 8), we determine Rouse number for each grain size measured in our domain (Figure 9).

3 Results

3.1 Time Lapse Elevation Maps and Sediment Flux

Using time lapse elevation scans taken periodically during the duration of each experiment, bedload flux was quantified by calculating the single bedform translating in each experiment. As an example, the time lapse surface of Experiment 2 is

https://doi.org/10.5194/egusphere-2026-5873
Preprint. Discussion started: 18 November 2026
© Author(s) 2026. CC BY 4.0 License.

presented in Figure 4. Bedload flux (m^2/s) is calculated as a function of the area translated between the horizontally averaged bedform profiles.

$$q_b = (1 - \lambda)A/t, \tag{9}$$

where λ is the bedform porosity (assumed to be 0.3), A is the translated area (m^2), calculated with the brinkline and lee-toe locations from scan to scan, and t is the time between scans (s).

In all the experiments the flux measured from the translation of the bedform decreases as the bedform translates. We note that the flux used in our shear stress calculations in the Discussion section is the average flux from the last 60 minutes of each experiment's duration. Each bedform developed from plane bed, and into a translating bedform (Figure 4). In the high flow conditions, this only occurred in the final hour, and to be broadly comparable across all conditions, we used this time duration for measuring flux.

3.2 Magnetic Concentration Profiles

The concentration profile of dense, magnetic sand particles is a function of the relative vigor of bulk transport (Figure 5). To make the experiments comparable, the final, measured concentrations are normalized against the initial concentration of magnetic sand to quartz, 1:90 by mass, and are reported as C_f/C_i, a dimensionless quantity. Values over one represent relative enrichment to the initial concentration or preferential accumulation. Values below one are depletion, or local winnowing.

"Lag," in the context of these experiments is defined as relative concentration enrichment of dense tracer grains behind the center of mass of the bedform in the experimental domain. This behavior is observable in all panels of Figure 5, except for Experiment 2, which is potentially a sampling issue. Relative concentration enrichment indicates preferential accumulation but does not establish the formation of a lag deposit (Experiments 2 and 8 crestlines).

The lowest flow condition, Experiment 5, has a strong lag behavior at the upstream end of the stoss slope, almost double the initial concentration. Within the body of the dune up to the lee face, the concentration is approximately 30% greater than the initial concentration. At the lee face, the concentration decreases below the initial concentration to 40%.

The low flow conditions, Experiments 4 and 6, have a strong lag at the upstream end of the bedform, 2.3 times greater than their initial concentration value, decreasing to equal to the initial concentration within the bedform in Experiment 4. In Experiment 6, the concentration decreases within the body of the bedform to as low as 70% of the original. In both experiments the concentration of magnetic particles decays to 30% and 40% of the original concentration beyond the dune.

The medium flow conditions, Experiments 3 and 7, also display a lag at the upstream end of the bedform. Within the bedform, the concentration is approximately equivalent to the original in Experiment 3. The concentration decreases to near the initial concentration in Experiment 7. Both have a strong depletion beyond the lee face to less than 50% of the initial concentration.

The high flow conditions, Experiments 2 and 8, have different lag behaviors than the other experiments. Experiments 2 and 8 have qualitatively different curves from one another: Experiment 2 has no lagged tail, though there is no data behind the last point. Experiment 8 has a very strong concentration enrichment behind the dune. Both however, have steady concentrations within the body of the dune itself. Experiment 2 has a 25% depletion, while Experiment 8 is only 10% depleted. Both have an

https://doi.org/10.5194/egusphere-2026-5873
Preprint. Discussion started: 18 November 2026
© Author(s) 2026. CC BY 4.0 License.

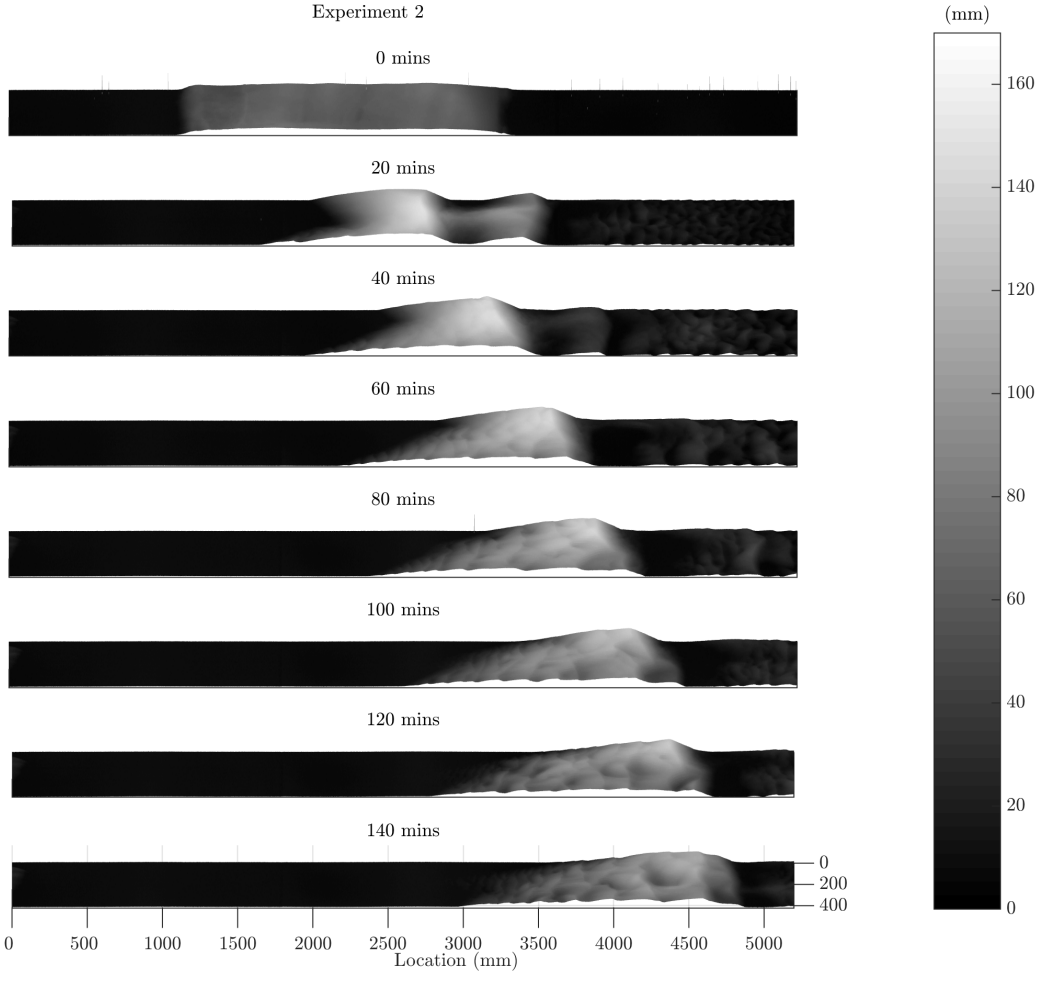


Figure 4. Time lapse elevation maps taken with a Keyence laser altimeter. The sediment was initially deposited as a plane bed $1-3\,m$ from the inlet and allowed to transport until all the sediment has moved past its initial deposition site, ensuring all sediment has been transported.

https://doi.org/10.5194/egusphere-2026-5873
Preprint. Discussion started: 18 November 2026
© Author(s) 2026. CC BY 4.0 License.

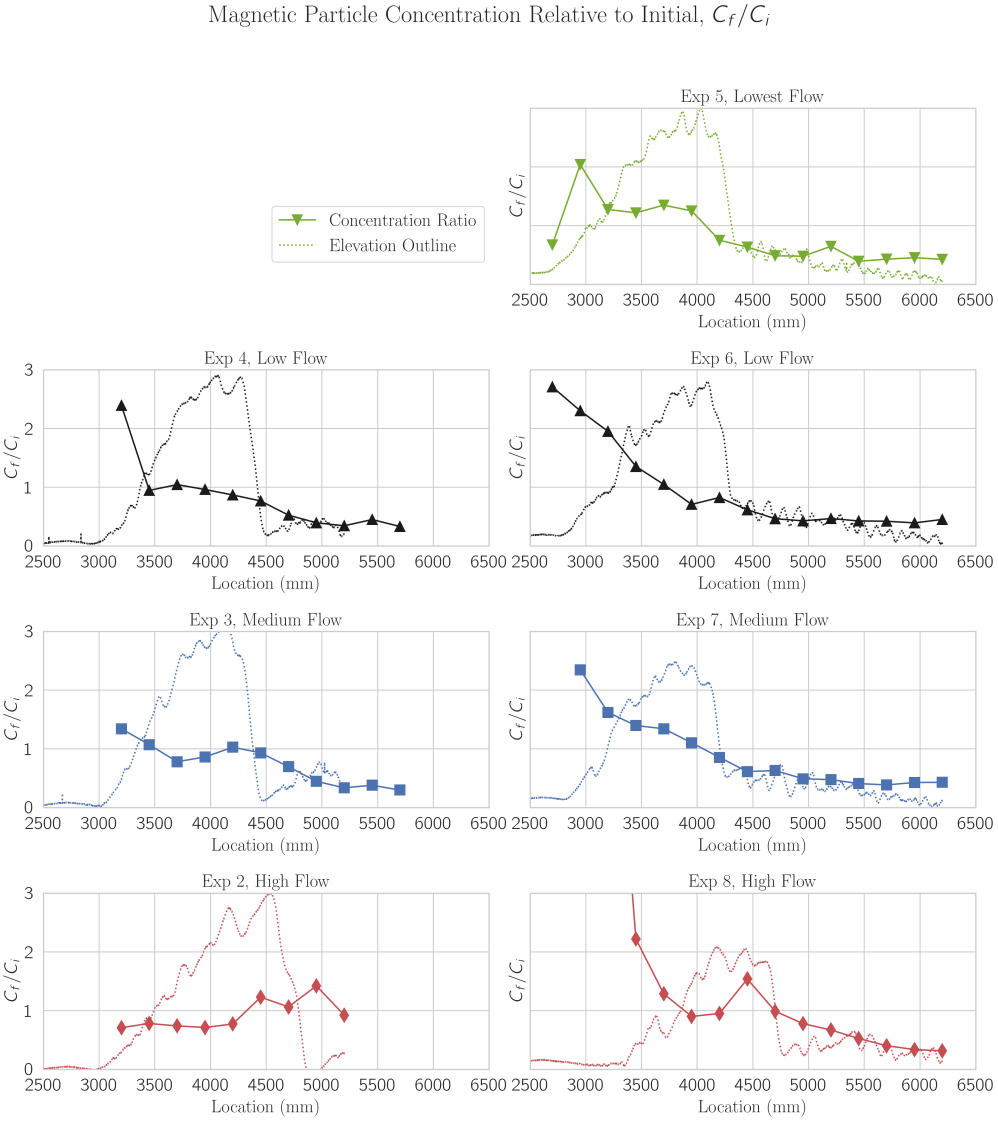


Figure 5. The mass concentration relative to the initial (1:90 by mass) of magnetic sediment along the length of the deposit. The deposit outlines are in the dotted lines. All runs have a concentration enrichment lag at the rear end of the dune, except Experiment 2. Experiments 2 and 8, the high flow runs, have a concentration enrichment around the crestline, due to dune deflation from quartz suspended sediment transport, which leaves the dense sediment behind. Note in the bottom right panel there is a concentration value that is extremely high and is off axis ($C_f/C_i \sim 8.27$)

https://doi.org/10.5194/egusphere-2026-5873
Preprint. Discussion started: 18 November 2026
© Author(s) 2026. CC BY 4.0 License.

enrichment of magnetic material at the dune crest of 28% and 53%. In Experiment 8, there is depletion at and beyond the lee face to 30% of the original. Experiment 2 has approximately the original concentration at the lee face and immediately beyond it.

3.3 Grain Size and Sorting

3.3.1 Quartz Sand

In all the experiments, the quartz grain size within the bedform approximates the original distribution (Figure 6). Beyond the lee face, the median grain size decreases.

The grain sorting, σ, is calculated using the Folk and Ward (1957) method,

$$\sigma = \frac{\Phi_{84} - \Phi_{16}}{4} + \frac{\Phi_{95} - \Phi_5}{6.6}, \tag{10}$$

where Φ_n is the nth percentile of the grain size distribution in the Wentworth Scale ($\Phi = -log_2 \frac{D}{D_0}$). In all experiments, quartz grain sorting remained somewhat constant over the domain at the threshold of "Well Sorted" to "Very Well Sorted" ($\sigma = 0.35$, Figure 7).

3.3.2 Magnetic Sand

The median magnetic sediment grain size (input: $D_{50mag} = 330\mu m$), had a similar grain size trend as quartz in the downstream direction (Figure 8). The median grain size remains constant within the body of the bedform and decreases beyond the lee face. Experiments 2 and 8 are the exceptions: Experiment 2 coarsens at the crestline, and Experiment 8 stays constant in the measured domain.

The sorting behavior of magnetic sand is different than the quartz sand (Figure 7). While sorting remained somewhat constant for all the quartz samples in all the experiments, the magnetic sand had variable results. The lowest flow condition, Experiment 5, is less well sorted at the crestline and lee face than in the rear of the dune, and subsequently becomes better sorted beyond the dune at the threshold of "Well Sorted" to "Very Well Sorted."

The low flow conditions, Experiments 4 and 6, improve their sorting along the length of the bedform, crossing the threshold to "Very Well Sorted." Beyond the lee face, sorting improves in Experiment 4. Experiment 6 maintains its sorting beyond the lee face.

The medium flow conditions, Experiments 3 and 7, maintain their sorting within the bedform. Beyond the lee face, the two experiments' behavior deviates slightly. Both have better sorting behind the crestline, approximately $0.75\,m$ from the lee face, but the sorting in Experiment 7 returns to that measured within the bedform, while the sorting in Experiment 3 becomes better with distance from the lee face.

In high flow conditions, Experiment 2, sorting is poorer than that measured in the other experiments, though it similarly improves along the length of the bedform starting at "Moderately Sorted" at the rear, becoming "Well Sorted." The sorting in Experiment 8 is consistently "Well Sorted" in the bedform and beyond the lee face.

https://doi.org/10.5194/egusphere-2026-5873
Preprint. Discussion started: 18 November 2026
© Author(s) 2026. CC BY 4.0 License.

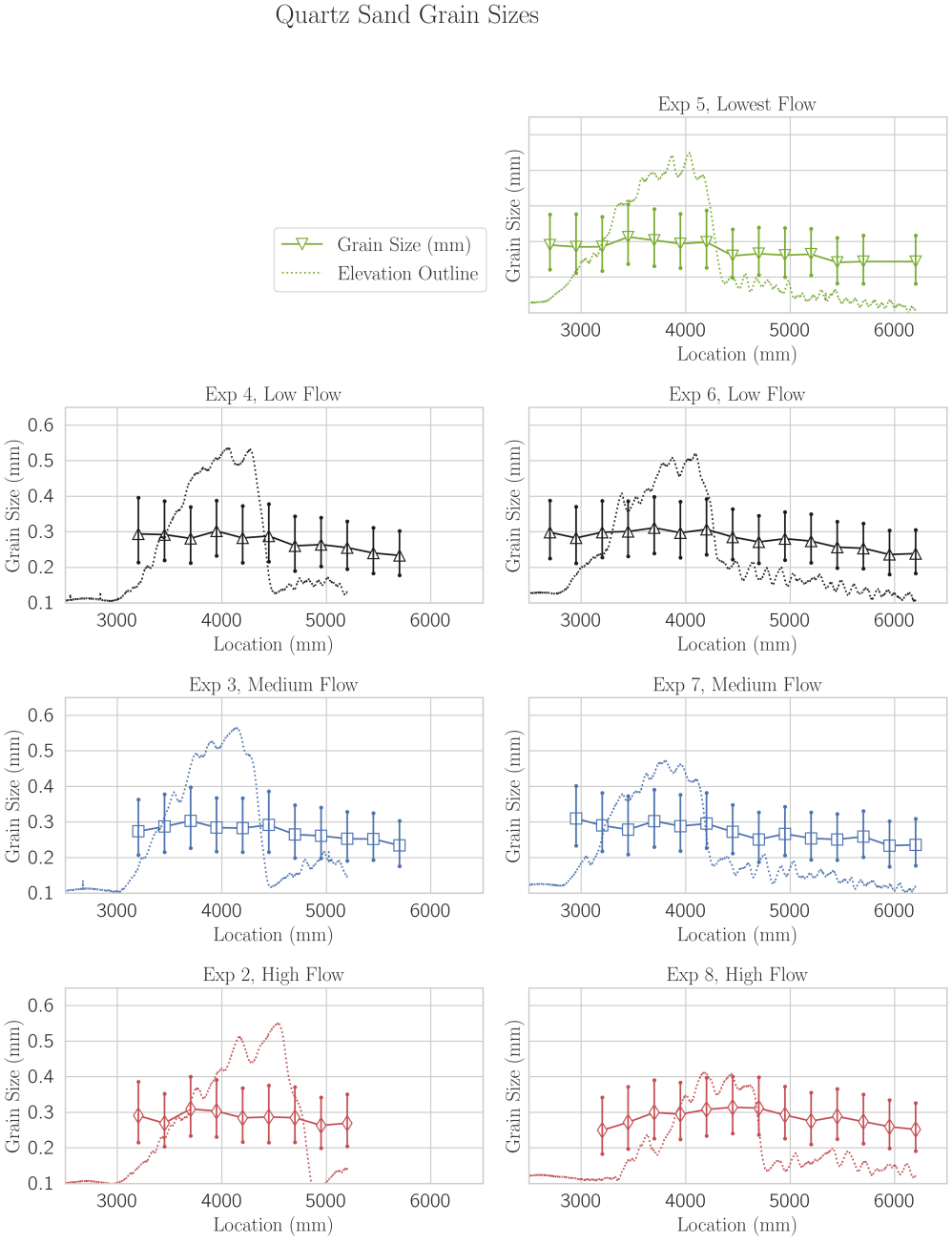


Figure 6. Quartz grain size data taken after each experiment. The markers represent the D_{16}, D_{50}, and D_{84}. The outline of the bedform where the samples were taken is the dotted line.

https://doi.org/10.5194/egusphere-2026-5873
Preprint. Discussion started: 18 November 2026
© Author(s) 2026. CC BY 4.0 License.

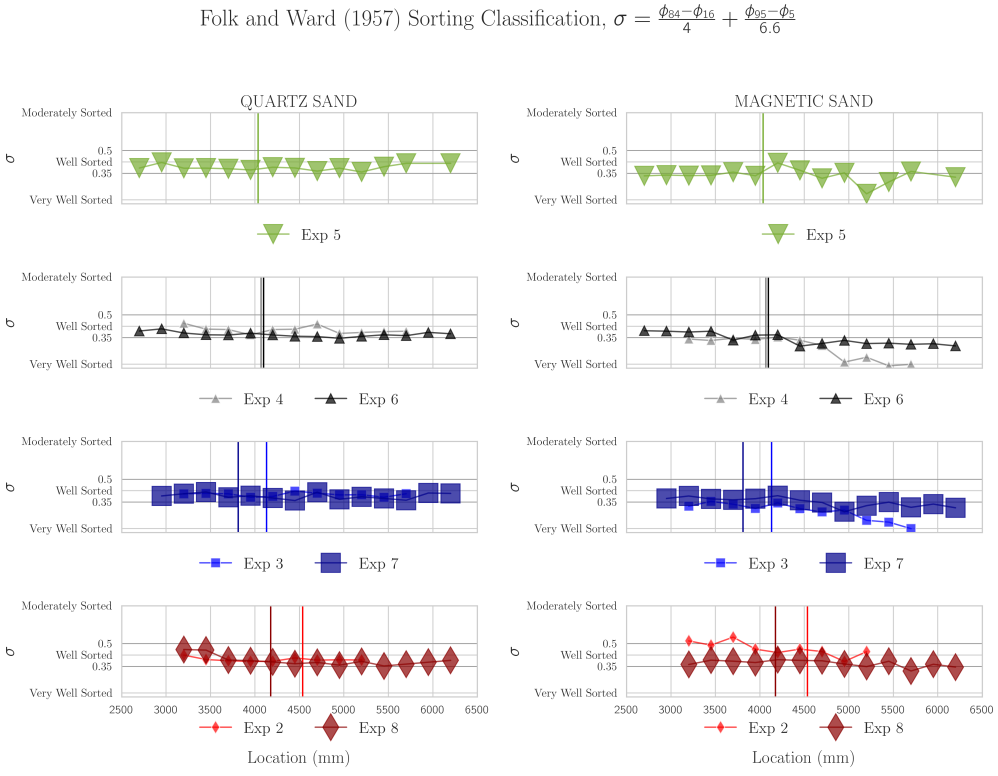


Figure 7. Folk and Ward (1957) sorting classification of sediment samples (Figure 6 and Figure 8), derived using Equation 10. The bedform crest lines are indicated by the vertical lines corresponding to the same color and shading for each experiment.

4 Discussion

From experiment to experiment, we observe different transport outcomes for the two sediment types. In low flow experiments, the dense tracer particles mostly lag at the rear of the dune. In the high flow experiments, the tracers are enriched at the crestline. To determine the transport conditions at the grain scale, we present an inverse model to calculate the stress required to transport the bedform. We then determine the suspension propensity for our two types of grains, and discuss these grain-scale parameters in the context of a bedform-scale analysis of the types of lag observed.

Our contribution is the direct observation that this contrast produces predictable, position-dependent dense-mineral enrichment, even within a single migrating bedform. This has consequences for where provenance samples should and should not be collected, which is discussed below.

4.1 Suspended Sediment Potential and Escape from the Bedform

We can combine our inverse model-derived shear velocities and the calculated settling velocity from each particle within the known frequencies of those grain sizes and determine a cumulative frequency distribution for the Rouse number (Figure 10).

https://doi.org/10.5194/egusphere-2026-5873
Preprint. Discussion started: 18 November 2026
© Author(s) 2026. CC BY 4.0 License.

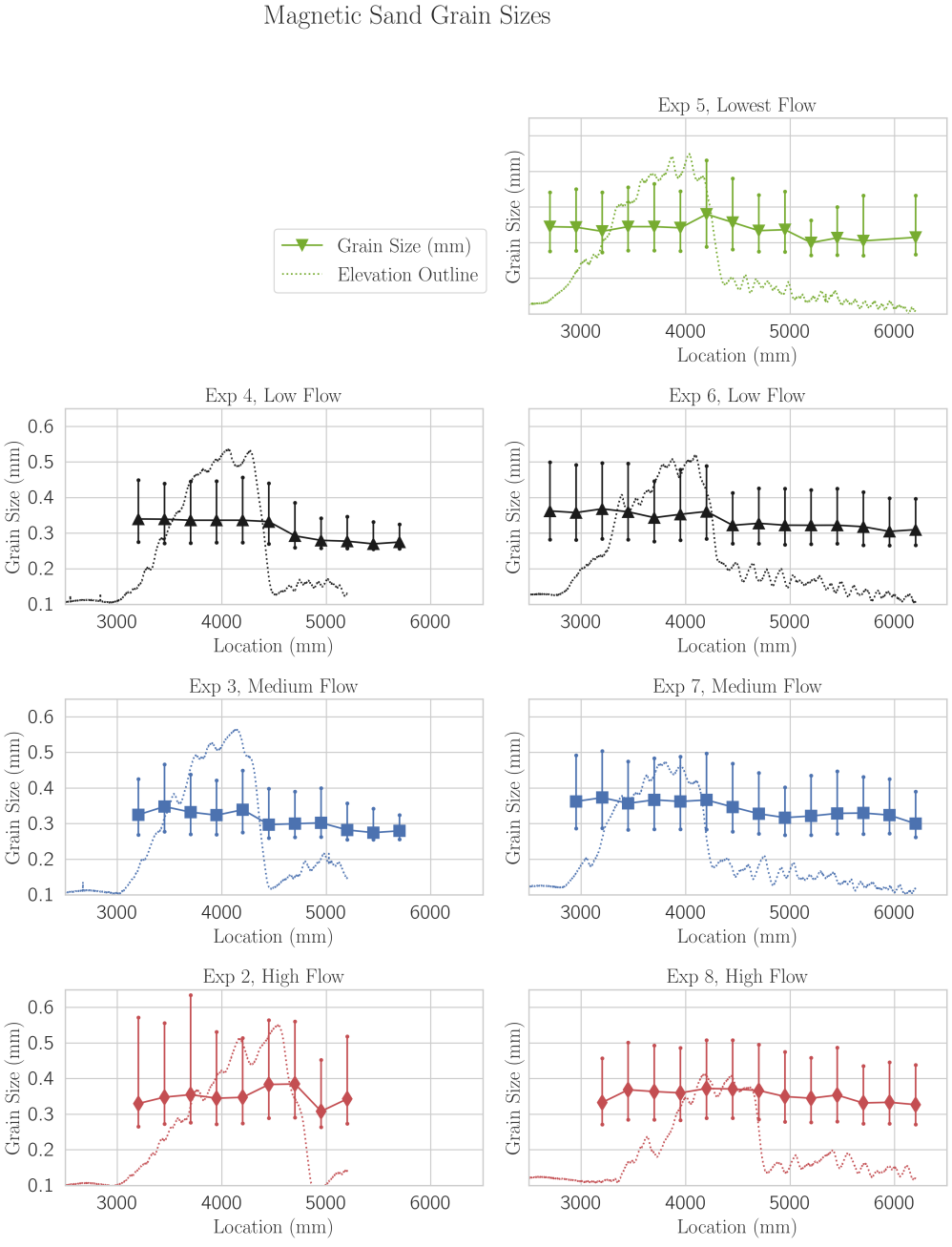


Figure 8. Magnetic sediment grain size data taken after each experiment. The markers represent the D_{16}, D_{50}, and D_{84}. The outline of the bedform is the dotted line.

https://doi.org/10.5194/egusphere-2026-5873
Preprint. Discussion started: 18 November 2026
© Author(s) 2026. CC BY 4.0 License.

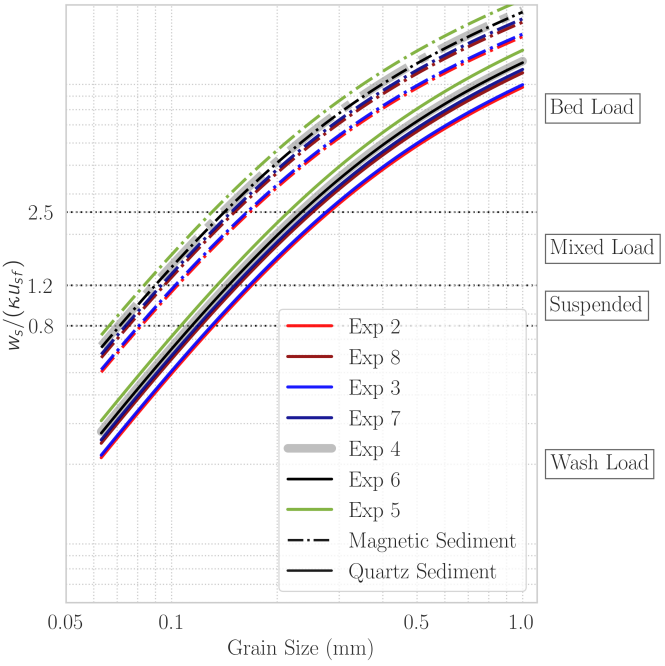


Figure 9. Based on the initial grain-size range, the ratio of the grain settling velocity and skin friction shear velocity for each experiment is computed for both quartz and magnetic sediments. The smooth lines are the quartz sediment, and the stippled lines are the magnetic sediment

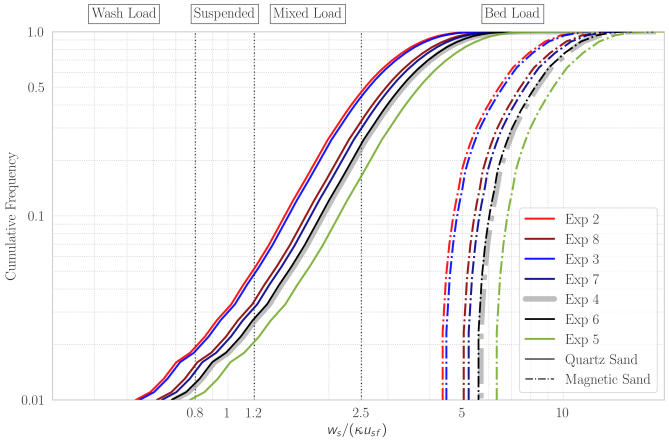


Figure 10. The Rouse Numbers of each experiment, derived from the initial grain size distribution of the two sediment types. The shear velocity for each experiment was determined by using the shear required to transport the bedform in each experimental condition. The smooth lines are the quartz sediment, and the stippled lines are the magnetic sediment.

https://doi.org/10.5194/egusphere-2026-5873
Preprint. Discussion started: 18 November 2026
© Author(s) 2026. CC BY 4.0 License.

Using the threshold of $\frac{w_s}{\kappa u_{sf}} < 2.5$, for incipient grain suspension, and $\frac{w_s}{\kappa u_{sf}} < 1.2$, as the threshold for full suspension (Bagnold, 1966; Nishimura and Hunt, 2000; Niño et al., 2003), we compare these calculated values to our experimental results. In every experiment, the threshold for full suspension ($\frac{w_s}{\kappa u_{sf}} < 1.2$) is not met for magnetic sediment. As discussed in the Methods section, despite a modest range in mean flow velocities between experiments, we were able to generate a range of sediment transport conditions because our inputs were near threshold for different styles of transport.

Bulk quartz sediment is in a mixed transport regime: the high flow and medium flow have almost 30 to 50 percent of grain sizes with a propensity for suspension ($\frac{w_s}{\kappa u_{sf}} < 2.5$), and the lowest flow only has 10 percent.

In all experiments, excluding the high flow Experiments 2 and 8, the magnetic sediment lags at the rear of the dune (Figure 5). In these cases, quartz sediment volume retention in the bedform is relatively high, over 95%, with the exception of Experiments 7 and 5 (Table 1). In contrast, the high flow experiments have a greater degree of sediment escaped from the bedform, approximately 10-20 percent. The greater loss of material from the high-flow bedforms is consistent with stronger transport and a larger contribution from the finer, more mobile quartz fraction. Further, as evidenced by the excess transport values of the median grain size ($(u_{sf}/u_c)^2 - 1$, Table 1), the magnetic sediment is in a lower transport regime than bulk sediment.

In these experiments, equivalence between dense tracers and bulk sediment has to be defined relative to a specific transport fraction: either the migrating bedform–bedload fraction, the suspended fraction, or the integrated bulk load (the weighted average of all types of sediment transport). This distinction is necessary because quartz grains may be advected from the bedform as suspended load while most dense tracer grains remain within or near the migrating bedform. Dense tracers can therefore keep pace with the bedform-preserved bedload component without actually keeping pace with the total quartz flux in the system.

To summarize, the sediment suspension model indicates that bulk quartz grains transport vigorously as bedload, and a non-negligible fraction have the propensity for full suspension in the experiments with high flow, which is borne out by the measured lost volume in the experimental bedforms (Figure 10, Table 1). The bedform still translates as a bedload structure while quartz also has substantial potential for suspension, especially in the higher-flow runs. The median magnetic grains are predicted to remain bedload-dominated in every experiment. The concentration profile of the magnetic sediment in the high flow cases indicates strong transport by the magnetic sediment, keeping pace with the bedload component of bulk sediment transport, though that does not account for the volume of quartz lost to escaped or suspended load. In the higher-flow experiments, dense tracers enriched near the crestline appear to keep pace with the bedform-scale, bedload component of quartz transport. Once the escaped fraction is included, dense tracer grains do not keep pace with the full quartz sediment load. The high flow experiments only show a reduction in dense-grain lag relative to the bedload fraction, but not complete equivalence with the total bulk sediment flux. Some magnetic particles are able to be transported beyond the bedform as escaped load, but as the depleted concentration profiles beyond the crestline indicate, they are a small fraction of the magnetic sediment ensemble.

https://doi.org/10.5194/egusphere-2026-5873
Preprint. Discussion started: 18 November 2026
© Author(s) 2026. CC BY 4.0 License.

4.2 Where in a bedform are dense tracers least decoupled from bulk style sediment transport?

The relationship between the similarity of grain-scale parameters like transport style and the observed concentration profile of dense grains within the dune can be used diagnostically. Starting with the concentration profile of dense tracers in a preserved bedform, one can deduce the degree to which bulk sediment and dense tracers were moving at similar rates.

The two patterns of dense-grain accumulation observed in these experiments are enrichment behind the bedform when bulk sediment moves predominantly as bedload, or “lag", and enrichment near the crestline when a larger fraction of the quartz population approaches suspension (Figure 5). In the first set of cases, bulk sediment moves as bedload and magnetic sediment also moves as bedload, but with a smaller excess shear stress relative to its critical threshold (Experiments 5, 4 and 6, Figure 10, Table 1). In these experiments, the transport of the quartz and magnetite grains led to a demixing of the original sediment bed. Despite a nominally similar transport type there is a substantial lag behavior, leading to high concentrations at the rear of the dune. In our experimental domain the lagging grains are exposed on a non-erodible bed, and are collected at the trailing edge of the dune’s stoss-side. In a train of dunes with an erodible bed, those grains would be trapped in a dune trough, leading to at least temporary burial (Figure 1). Once that happens, those buried grains become part of the geologic record, and are not transported at the timescale of a single event.

These observations suggest that dense-mineral samples should always be tied explicitly to their position within the preserved bedform structure for proper transport contextualization. In modern fluvial contexts, where an entire bedform is available for sampling, samples from a dune’s stoss-side or sourced from basal lag concentrations will most likely overrepresent preferentially accumulated, coarse, dense grains. Samples from near the lee face or immediately downstream will most likely capture the fine, mobile fraction that escaped the bedform, but this fraction is not representative of the dense-mineral population as a whole in terms of size or transportability. In bedforms generated by more vigorous transport, crestline-enriched dense grains are the best candidates for comparing with the bedload fraction of the quartz sediment, but they should not be treated as equivalent to the escaped, suspended quartz load. In stratigraphic contexts, where the lee faces of the dune are what are primarily preserved, the best effort to estimate the mid-dune elevation must be made. Samples taken from near the base of the lee face will be preferentially enriched in the buried, lagged grains from bedforms ahead. The ideal location is the middle height of the lee face, which would most represent the median grain.

If we compare the grain-size distributions of the lagged and escaped magnetic fractions, we observe that transport across a single bedform does not only redistribute dense grains spatially, but fractionates the tracer population itself. Figure 11 shows that the grains transported beyond the bedform are finer than both the lagged fraction and the input distribution, while the lagged grains more closely resemble the original tracer population and that of the bedform, though the reconstructed distributions all have measurable differences in their two-sample Kolmogorov-Smirnov comparisons (Massey Jr, 1951). Running tests between all populations for each experiment results in a rejection of the null hypothesis that the samples come from the same distribution at a significance of $p << 0.01$ (the D-values are reported in Daniller-Varghese et al. (2026)). These p-values are approximate because the effective grain counts are inferred from measured masses rather than obtained from direct particle counts. This indicates that the migrating bedform acts as a selective filter on dense grains. Coarser grains are preferentially retained within or

https://doi.org/10.5194/egusphere-2026-5873
Preprint. Discussion started: 18 November 2026
© Author(s) 2026. CC BY 4.0 License.

behind the bedform, while only the finer tail of the dense grain population is able to escape. When considered alongside Figure 10, this pattern is mechanically consistent with the much lower suspension propensity of the dense grains relative to the quartz sediment. Only a small fraction of the finest dense grains approach transport behavior comparable to the more mobile quartz fraction, though still remaining in the bedload-dominant regime, while the coarser dense grains are increasingly decoupled from bulk-sediment transport and are more likely to be lagged in the experiment, and buried in a natural context. In provenance terms, this means that a bedform does not preserve a single faithful record of dense tracer mobility. Instead, different positions within the same bedform preserve different subsets of the tracer population.

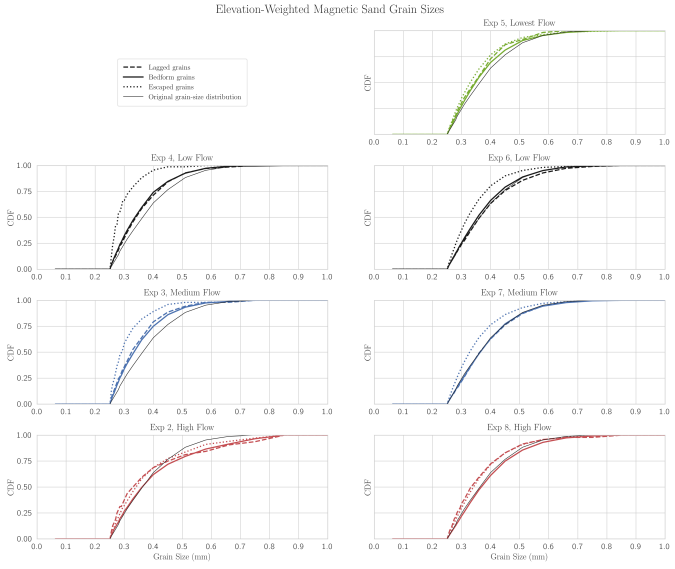


Figure 11. The cumulative distribution functions of the elevation-weighted distributions of the lagged grains (dashed lines), bedform grains (bold lines), and escaped (dotted lines) grain size distributions of the magnetic sediment. The original distribution is the fine line. Testing whether any combinations of the samples come from the same distribution using a two-sample Kolmogorov-Smirnov Test rejects the null hypothesis: the distributions are all statistically distinct from one another.

The dense grains that may transport at the same rate as their quartz neighbors are those traveling in escaped, suspended load, bypassing the dunes, though they represent a small fraction of total transport. As we observed, the escaped, suspended load fraction of dense grains is finer and better sorted than those grains in the bedform (Figure 7). It is likely that those grains with similar settling velocities have comparable speeds, but they are not representative of bulk transport.

Only a very small fraction of the dense tracer grain population reflects the suspended load transport in every experiment (Figures 8, 11). To effectively sample them, they must be picked at the base of the lee face of a dune near the surface, and are only comparable to grains in a similar location, and not within the body of the bedform. This ensures that they are not compared with exhumed grains that were previously captured and buried.

In the case of high flow transport, where sampling reveals enrichment of dense, coarse sediment at the crestline, those dense grains do travel at the same rate as bulk bedload sediment, though not at the same rate as the escaped fraction. This is provided

https://doi.org/10.5194/egusphere-2026-5873
Preprint. Discussion started: 18 November 2026
© Author(s) 2026. CC BY 4.0 License.

that there is not too much loss to suspended load, though the presence of bedforms is a helpful guide in that regard. A fully suspended load dominated regime would transition to upper plane bed (Paola et al., 1989). In this case, if one assumes that most sediment in source to sink scenarios moves as bedload, even under vigorous transport conditions, then the dense tracer minerals at the crestline transport at the same rate as their neighboring quartz grains.

One can also examine the dense tracer grains that are transported in suspended load. While grains in suspended load are comparable in terms of their calculated settling velocities, only a small percent of the overall distribution is representative of this behavior, as in the low flow cases. In the case where bulk sediment transport is primarily in bedload, the grains at the base of the lee face are the comparable escaped fraction.

Practically, provenance sampling would benefit from consideration of depositional position. Samples should be collected from discrete structural positions and should be treated as separate transport populations: in the modern lag-rich stoss, crestline concentrations, lee-face deposits, and any finer escaped fraction are all distinct; in strata, the upper and lower preserved lee faces should be carefully parsed as escaped, enriched, or lagged grains. Comparing these populations within the same bedform may be more informative than combining them into a single provenance sample, because each position records a different degree of transport filtering.

4.3 Experimental scope and implications for natural systems

Our domain, while large, is still constrained, and required the experimental cutoff to be one bedform translation. This means that our analysis was limited to dense-grain partitioning over the smallest possible bedform scale, rather than a cumulative downstream dispersion over many bedforms. This means that the escaped fraction identifies the grains capable of leaving the bedform over the compact experimental interval, but does not provide a direct measurement of long-term travel distance or particle velocity. Future work will use a longer flume, and investigate the effects over many bedforms. Second, the analysis emphasizes periods of steady bedform translation, and isolates the mechanics of bedform-scale sorting but omits transient adjustment, scour, and reworking that always occur in natural flows. These choices make the experiments conservative tests of bedform-scale filtering, and are informative for interpreting concentration behaviors, but these experiments do not provide a universal rate law for zircon travel timing.

5 Conclusions

In this study, we examined the transport lag of dense particles relative to ambient sediment as an analogue for the behavior of detrital zircons in fluvial transport. Our experiments show that dense tracers and bulk quartz sediment can become decoupled over the scale of a single migrating bedform, and that the degree of decoupling is a function of sediment transport regime. In bulk-sediment bedload-dominated cases, dense grains preferentially lag at the stoss side of the dune, whereas in higher-flow cases where a larger fraction of the quartz population has suspension potential, dense grains are enriched nearer the crestline, where quartz is more readily lost from the bedform.

https://doi.org/10.5194/egusphere-2026-5873
Preprint. Discussion started: 18 November 2026
© Author(s) 2026. CC BY 4.0 License.

The experiments also show that dense grains are not uniformly distributed within a single bedform. Their concentration and grain-size distributions vary with position in the bedform. The grains transported beyond the bedform are finer than the lagged fraction and finer than the initial dense-grain distribution, indicating that transport across even one bedform selectively exports the finer tail of the dense tracer population while retaining coarser grains as lag. Bedform migration therefore filters the dense-grain population into distinct subpopulations.

These results have a direct implication for detrital zircon sampling. Dense tracers should not be assumed to represent the bulk sediment simply because they occur beside quartz grains in the same deposit. Instead, the representativeness of a dense-tracer sample depends on where within the depositional structure it is collected, and on whether the sampled grains belong to the lagged, retained, or escaped fraction. In lower-flow, bedload-dominated settings, coarse dense grains concentrated in stoss-side lag deposits are least likely to reflect the actively transported bulk sediment, whereas finer dense grains near the lee face may better approximate the more mobile fraction. In higher-flow bedforms that retain clear relief, dense grains enriched near the crestline may best approximate the co-moving bedload fraction of the bulk sediment.

Our experiments represent a simplified transport system, and we do not directly measure particle travel times, hop velocities, or zircon transport itself. Accordingly, our results do not provide a universal zircon-to-quartz conversion rule. Rather, they provide a physically grounded framework for understanding how bedforms sort dense tracers relative to bulk sediment, and for identifying the parts of a deposit where dense grains are most and least likely to approximate the transport behavior of the surrounding sand.

More broadly, these experiments show that bedform-scale transport can bias the dense-mineral signal preserved in sedimentary deposits over short spatial and temporal scales. Provenance interpretations based on detrital zircons should therefore consider depositional structure and transport sorting explicitly, rather than assuming that all zircons within a bed equally represent the bulk sediment in transport.

Code and data availability. The data and analysis code are available through Zenodo under a CC BY 4.0 license: Daniller-Varghese et al. (2026), Bedform Experiments Conducted at the University of Texas at Austin, 2018, https://doi.org/10.5281/zenodo.19455484. The authors confirm that the data supporting the results and conclusion of this study are available within the article and the repository.

Author contributions. Max S. Daniller-Varghese: Conceptualization, Data curation, Formal analysis, Investigation, Methodology, Project administration, Resources, Software, Validation, Visualization, Writing - Original Draft, Writing - Review & Editing; David C. Mohrig: Conceptualization, Formal analysis, Funding acquisition, Investigation, Methodology, Project administration, Resources, Supervision, Validation, Visualization; Wonsuck Kim: Conceptualization, Funding acquisition, Investigation, Methodology, Project administration, Resources, Supervision, Visualization.

Competing interests. The authors declare that they have no conflict of interest.

https://doi.org/10.5194/egusphere-2026-5873
Preprint. Discussion started: 18 November 2026
© Author(s) 2026. CC BY 4.0 License.



Acknowledgements. The Authors gratefully acknowledge funding from the UT-CSM RioMAR Consortium, and the Jackson School of Geosciences Chair. OpenAI ChatGPT was used to assist with figure typesetting and layout. All scientific content, interpretation, and final presentation decisions were made by the authors.

https://doi.org/10.5194/egusphere-2026-5873
Preprint. Discussion started: 18 November 2026
© Author(s) 2026. CC BY 4.0 License.

References

Bagnold, R. A.: An approach to the sediment transport problem from general physics, US government printing office, 1966.

Coutts, D. S., Matthews, W. A., and Hubbard, S. M.: Assessment of widely used methods to derive depositional ages from detrital zircon populations, Geoscience Frontiers, 10, 1421–1435, https://doi.org/10.1016/j.gsf.2018.11.002, 2019.

Daniller-Varghese, M., Mohrig, D., and Kim, W.: Bedform Experiments Conducted at the University of Texas at Austin, 2018, https://doi.org/10.5281/zenodo.19455484, data set, 2026.

Dietrich, W. E.: Settling velocity of natural particles, Water resources research, 18, 1615–1626, 1982.

Dobbs, S. C., Malkowski, M. A., Schwartz, T. M., Sickmann, Z. T., and Graham, S. A.: Depositional controls on detrital zircon provenance: An example from Upper Cretaceous strata, southern Patagonia, Frontiers in Earth Science, 10, 824 930, 2022.

Fedo, C. M., Sircombe, K. N., and Rainbird, R. H.: Detrital zircon analysis of the sedimentary record, Reviews in mineralogy and geochemistry, 53, 277–303, 2003.

Ferguson, R. I. and Church, M.: A simple universal equation for grain settling velocity, Journal of sedimentary Research, 74, 933–937, 2004.

Folk, R. L. and Ward, W. C.: Brazos River bar [Texas]; a study in the significance of grain size parameters, Journal of Sedimentary Research, 27, 3–26, 1957.

Garzanti, E., Andò, S., and Vezzoli, G.: Grain-size dependence of sediment composition and environmental bias in provenance studies, Earth and Planetary Science Letters, 277, 422–432, 2009.

Gehrels, G.: Detrital zircon U-Pb geochronology applied to tectonics, Annual Review of Earth and Planetary Sciences, 42, 127–149, 2014.

Ibañez-Mejia, M., Pullen, A., Pepper, M., Urbani, F., Ghoshal, G., and Ibañez-Mejia, J. C.: Use and abuse of detrital zircon U-Pb geochronology case from the Río Orinoco delta, eastern Venezuela, Geology, 46, 1019–1022, 2018.

Lawrence, R. L., Cox, R., Mapes, R. W., and Coleman, D. S.: Hydrodynamic fractionation of zircon age populations, Bulletin, 123, 295–305, 2011.

Malkowski, M. A., Sharman, G. R., Johnstone, S. A., Grove, M. J., Kimbrough, D. L., and Graham, S. A.: Dilution and propagation of provenance trends in sand and mud: Geochemistry and detrital zircon geochronology of modern sediment from central California (USA), American Journal of Science, 319, 846–902, 2019.

Massey Jr, F. J.: The Kolmogorov-Smirnov test for goodness of fit, Journal of the American statistical Association, 46, 68–78, 1951.

Mohrig, D. and Smith, J. D.: Predicting the migration rates of subaqueous dunes, Water Resources Research, 32, 3207–3217, 1996.

Nelson, J. M. and Smith, J. D.: Mechanics of flow over ripples and dunes, Journal of Geophysical Research: Oceans, 94, 8146–8162, 1989.

Niño, Y., Lopez, F., and Garcia, M.: Threshold for particle entrainment into suspension, Sedimentology, 50, 247–263, 2003.

Nishimura, K. and Hunt, J.: Saltation and incipient suspension above a flat particle bed below a turbulent boundary layer, Journal of Fluid Mechanics, 417, 77–102, 2000.

Nittrouer, J. A., Mohrig, D., and Allison, M.: Punctuated sand transport in the lowermost Mississippi River, Journal of Geophysical Research: Earth Surface, 116, 2011.

Paola, C., Wiele, S. M., and Reinhart, M. A.: Upper-regime parallel lamination as the result of turbulent sediment transport and low-amplitude bed forms, Sedimentology, 36, 47–59, https://doi.org/10.1111/j.1365-3091.1989.tb00819.x, 1989.

Rouse, H.: Modern conceptions of the mechanics of fluid turbulence, Trans ASCE, 102, 463–505, 1937.

Saylor, J. E. and Sundell, K. E.: Quantifying comparison of large detrital geochronology data sets, Geosphere, 12, 203–220, 2016.

https://doi.org/10.5194/egusphere-2026-5873
Preprint. Discussion started: 18 November 2026
© Author(s) 2026. CC BY 4.0 License.



Sharman, G. R. and Malkowski, M. A.: Needles in a haystack: Detrital zircon U-Pb ages and the maximum depositional age of modern global sediment, Earth-Science Reviews, 203, 103 109, 2020.

Shields, A.: Application of similarity principles and turbulence research to bed-load movement, 1936.

Sircombe, K. N., Bleeker, W., and Stern, R. A.: Detrital zircon geochronology and grain-size analysis of a 2800 Ma Mesoarchean proto-cratonic cover succession, Slave Province, Canada, Earth and Planetary Science Letters, 189, 207–220, 2001.

Stokes, G. G.: On the effect of the internal friction of fluids on the motion of pendulums, vol. 9, Pitt Press Cambridge, 1851.

Udden, J. A.: Mechanical composition of clastic sediments, Bulletin of the Geological Society of America, 25, 655–744, 1914.

Vermeesch, P.: On the visualisation of detrital age distributions, Chemical Geology, 312-313, 190–194, https://doi.org/10.1016/j.chemgeo.2012.04.021, 2012.

Vermeesch, P.: Dissimilarity measures in detrital geochronology, Earth-Science Reviews, 178, 310–321, 2018.

Viparelli, E., Solari, L., and Hill, K.: Downstream lightening and upward heavying: Experiments with sediments differing in density, Sedimentology, 62, 1384–1407, 2015.

Wiberg, P. L. and Rubin, D. M.: Bed roughness produced by saltating sediment, Journal of Geophysical Research, 94, 5011–5016, https://doi.org/10.1029/JC094iC04p05011, 1989.